Advances in High Pressure Science & Technology
Edited by A.K.Singh
Tata McGraw-Hill, New Delhi

High Pressure - High Temperature Processing and Performance of wBN-cBN Composite Tools

C.Divakar, S.K.Bhaumik and A.K.Singh
Materials Science Division, National Aerospace Laboratories, Bangalore 560017

Abstract

The wurtzite phase of boron nitride (wBN) is obtained in large quantities by shock loading graphitic boron nitride (gBN). The sintering of wBN powder at high pressures and temperatures leads to the conversion of wBN to the cubic boron nitride phase (cBN). Compacts with varying amounts of cBN can be obtained by controlling the pressure, temperature and time. The wBN-cBN composites with 45-55 % cBN have hardness in the range 30-70 GPa, fracture toughness 13-16 MPa$\sqrt{m}$ and thermal conductivity 40-50 W m^{-1} K^{-1}. The composite has a hot hardness of about 20 GPa at 1400 K. The unique combination of high hardness and fracture toughness makes the composite tool capable of machining under interrupted conditions. The processing of wBN for cutting tool applications, the characterization of the tools and the performance of the composite tools in the machining of hardened steels (HRC 40-63), high nickel cast iron (BHN 120-160) and Ti-6Al-4V alloy (HV 310) are presented in this paper.

1 Introduction

The increasing demand for higher productivity and lower manufacturing costs of machined components has led to the development of newer cutting tool materials capable of operating at increased cutting speeds (Fig.1). The increase in productivity requires a compromise in the incompatible quantities, (a) larger and or faster metal removal rate, (b) long tool life and (c) required surface finish. The high cutting speed or high metal removal rate is associated with the generation of high temperature at the tool-work interface. Therefore, a cutting tool used should be resistant to fracture and plastic deformation. In addition, the wear resistance of the tool (a function of the tool-work combination and the temperatures generated during machining), is also

important. The commonly used tool materials such as cemented carbides, titanium carbide based cermets, and alumina based ceramic tools have a very short life and sometimes are unable to cut hardened steels, chilled cast irons, titanium alloys and super alloys (difficult-to-cut materials) because of tool deformation or edge fracture. The tungsten carbide tools which are commonly used in machining of steels and other alloys fail at high cutting speeds due to plastic deformation. The ceramic tools which have low fracture toughness, need rigid and stable machines. The difficult-to-cut materials are mostly shaped by grinding. A cutting tool expected to perform under severe machining conditions should therefore have adequate fracture toughness, high hot hardness, thermal shock resistance, and must be chemically stable and inert at the operating temperatures.

The advancement in high pressure technology has made it possible to develop a new generation of superhard materials based on diamond and cubic boron nitride[2–4]. In many situations, the final grinding operations of the difficult-to-cut materials can be replaced by turning operation with the tools made of these materials. The use of tools based on these materials have increased the cutting speeds by a factor of 100 over the turn of this century.

Diamond is the hardest material known, but the use of diamond tool is limited to nonferrous materials and ceramics because of its reaction with ferrous materials. Though the hardness of boron nitride is lower than that of diamond, the tools based on boron nitride have better thermal stability and chemical inertness with respect to iron. The diamond and boron nitride tools are complementary to each other in applications, in that, the diamond tools can cut all but ferrous alloys and boron nitride tools can cut all ferrous alloys.

The detailed reviews are available on the properties of cubic boron nitride[5] and its processing for cutting tool applications[6–8]. The polycrystalline boron nitride (PCBN) tools have performed well over the years in the machining of hardened steels and creep resistant alloys. But, the low fracture toughness of these tools imposes a serious limitation in their use under interrupted cutting conditions. Also the use of cBN tools requires vibration free rigid machines.

A composite tool based on the wurtzite and cubic modifications of boron nitride has been found to have better fracture toughness than that of PCBN tools, and perform well under interrupted cutting conditions[9–11]. They can also tolerate high

level of vibration in the machines. In this paper, the high pressure-high temperature processing of wBN for cutting tool applications , the properties of the tools, and their performance in machining hardened steels, cast irons and titanium alloys are presented.

2 Boron nitride : structure and phase diagram

Boron nitride exists in three different polymorphic forms : (i) hexagonal or graphitic (gBN), (ii) hexagonal wurtzitic (wBN) and (iii) the cubic zinc blende (cBN). Under ambient conditions, gBN is stable, and both wBN and cBN are the metastable phases. The crystallochemical characteristics of various phases of boron nitride are given in Table 1 .

Table 1: Crystallochemical characteristics of various modifications of boron nitride (Ref.12)

Modification	Coordination number	No. of atoms/ unit cell	*a* A°	*c* A°	*d* g cm^{-3}
gBN	3	4	2.504	6.661	2.29
wBN	4	4	2.55	4.23	3.50
cBN	4	8	3.615	-	3.51

The gBN structure is made up of plane hexagonal networks, each atom of one kind is surrounded by three atoms of the other. The layers are arranged one over the other. The wBN and cBN lattices are characterized by tetrahedral arrangements of atoms. The cBN lattice can be obtained by interpenetration of two fcc lattices, and the wBN lattice by a combination of two hcp lattices[13]. The crystal structures of both wBN and cBN consist of sp^3 hybridization, and therefore their mechanical properties are expected to be similar.

The conversion of gBN to wBN and cBN takes place under the application of high pressures and high temperatures. The gBN transforms to denser modifications at pressures over 10 GPa at and above room temperature without the aid of catalysts[14].

The phase diagram of boron nitride is shown in Fig 2. The dotted lines in the phase diagram delineate the gBN to metastable wBN or cBN and metastable wBN or cBN to stable gBN regions.

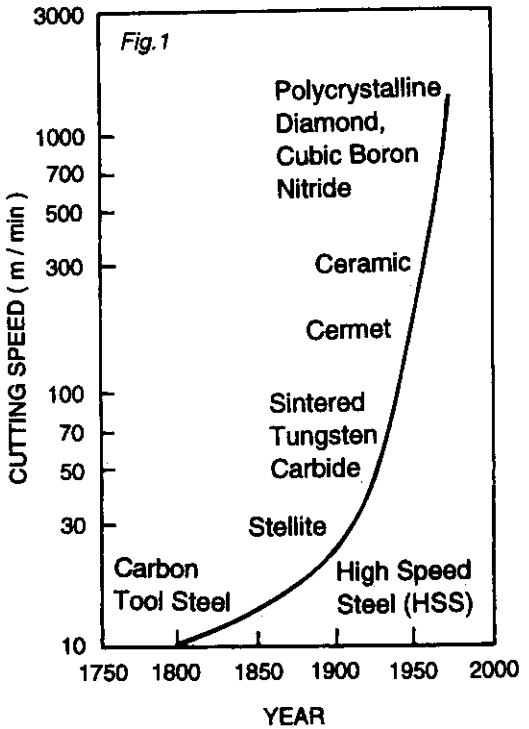

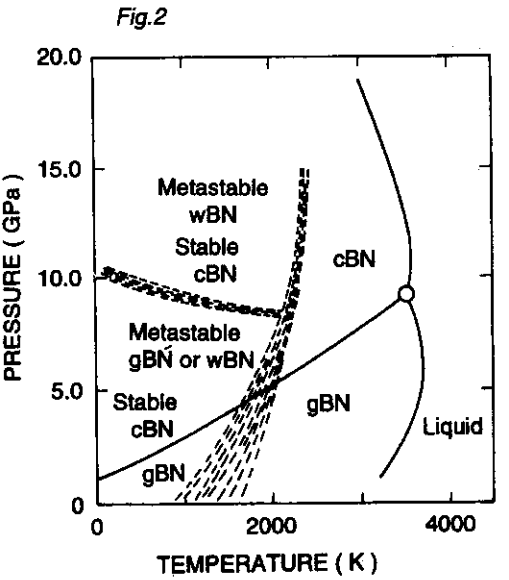

Figure 1: *Historical development of tool materials (Ref.1).*

Figure 2: *Phase diagram of boron nitride (Ref.15).*

The wBN does not form from gBN by direct or indirect processes up to 7 GPa. Around 8.5 GPa, wBN is formed marginally from gBN depending on the starting material and the reaction cell. Around 13 GPa, gBN transforms to wBN even at room temperature[15–19]. The wBN transforms completely to cBN around 2100^{0}C at pressures high enough to retain the stability of cBN. The wBN can also be obtained by static compression of gBN and a catalyst in presence of shear stresses [20], and the shock compression of gBN[21–31]. The conversion of gBN to cBN under static pressure

in presence of various catalysts is well known[32–37].

3 Processing of wBN for cutting tool applications

3.1 Large scale synthesis of wBN

As mentioned earlier, the wBN can be produced from gBN by three distinct methods: (a) the static compression of gBN at very high pressures, (b) static compression of gBN and a catalyst in presence of shear stresses and (c) the shock compression of gBN. The wBN is produced in large quantities by shock compression of gBN. For shock compression, the gBN powder is mixed with a metallic powder (Fe,Cu) and the mixture is contained in a stainless steel ampoule. The metallic powders are used to remove the heat generated during the shock treatment. The shock waves can be generated by (i) an explosive charge surrounding the sample and (ii) an impact of a metal plate or projectile accelerated by an explosion of charge or gas at high pressures. The shock Hugoniot and the pressure volume relation of boron nitride indicated a phase transformation around 12.2 GPa and 230^{0}C and this was identified to be associated with the gBN→ wBN transformation[21,22,24]. The fraction of wBN obtained after the shock compression depends on the crystalline state of the starting material, being higher for better crystallized material[23–29]. The rise in temperature during shock compression may lead to a partial wBN →gBN transformation. Thus, the shock recovered specimen may contain residual gBN phase (~3%). The electron microscopic studies on shock treated gBN samples have shown that, the orientation relationships $(001)_{gBN} \| (001)_{wBN}$ and $(110)_{gBN} \| (110)_{wBN}$ exist, and suggested that the gBN→ wBN is a diffusionless martensitic transformation [38].

The gBN and wBN after shock compression, have a highly defective structure. The high concentration of defects results in weakening the interatomic bonds and facilitates the diffusion process in the wBN→cBN transformation during sintering[39]. The amount of wBN obtained depends on the conditions under which the shock experiments are performed, but does not exceed 80-87% in absence of a catalyst. Under shock, gBN→wBN transformation is hindered by the comminution of gBN particles. The increase in the defect concentration destroys the crystallographic correlation between gBN and wBN. Also, depending on the temperature during the shock, some wBN is converted back to gBN. During the shock compression of gBN with a certain amount of water, the action of shock on the starting structure is weakened and the gBN→wBN transformation is promoted[40].

3.2 Stability of wBN at high temperatures

The wBN is a metastable phase under ambient conditions and transforms into the stable graphitic phase at elevated temperatures. The driving force for the transformation increases with the increase in temperature. The high mobility of atoms at elevated temperatures assists the transformation. The kinetics study of wBN→gBN transformation in vaccum under isothermal conditions at temperatures 700, 825 and 950^{0}C has shown that, the amount of gBN transformed increases initially with the annealing time and then attains a saturation value [41]. The transformation is controlled by the growth of the stable phase. The rate of the transformation depends on the number of nucleation centers capable of undergoing the transformation at a given temperature. If the phase transformation is to proceed further, the temperature must be increased in order to activate new centers. A complete conversion of the wBN to gBN takes place at ~1350^{0}C in about 30 minutes.

4 Fabrication of wBN based tools

The flow diagram for the fabrication of wBN based polycrystalline boron nitride tools is shown in Fig.3. The wBN powder obtained by shock treatment of gBN is sintered at high pressures and high temperatures to obtain the polycrystalline compacts. The sintering of wBN powder at high pressures are conducted using various apparatus like the Toroid[42], Belt[43], Tetrahedral[44] and Cubic anvil[45–47] type. These apparatus are capable of generating high pressures and temperatures and sustain them for required lengths of time. The Toroid type apparatus is economical in synthesizing compacts of 3 - 8 mm diameter and 5 mm long, which can be readily used as cutting tools.

The Toroid type high pressure chamber is shown in Fig.4. It comprises of two identical co-axially placed dies (made of tungsten carbide) one against the other. The dies have a lens like portion in the centre and concentric grooves on their working surfaces . The powder sample to be pressed is placed in the space between the central portions of the dies surrounded by a solid pressure transmitting medium. The samples are pressurized by loading the assembly with a high tonnage press. The Toroid apparatus is capable of generating pressures up to 10 GPa at 2300^{0}C with a working volume of ~0.5 cc.

For the production of the composite tool, the wBN powder is loaded in a graphite tube (heater) and is assembled in a gasket made of catlinit (a type of pyrophyllite).

The sample is heated by passing high current at low voltage through the graphite heater. The pressure calibration of the high pressure assembly were done using the resistance discontinuities at phase transitions in Bi I-II (2.54 GPa), Ba (5.8 GPa) and Bi III-V (7.7 GPa). The power temperature calibration were done by measuring the temperature inside the high pressure cell using a Pt - Pt 10% Rh thermocouple.

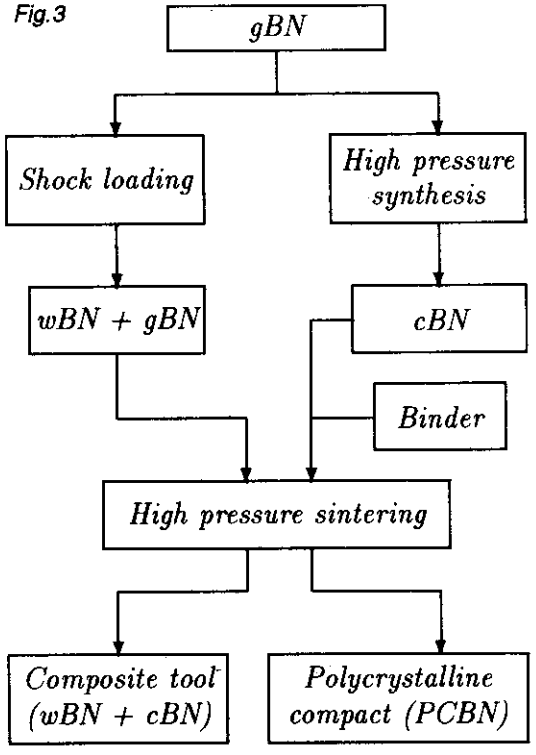

Figure 3: *Flow diagram for the manufacture of wBN based tools.*

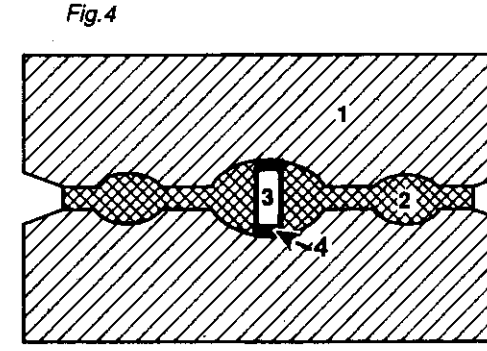

Figure 4: *Toroid type high pressure - high temperature apparatus (Ref.48).1. Tungsten carbide dies. 2. Catlinit. 3. Sample space. 4. Graphite heater.*

The sintering experiments were conducted in the pressure range 5.5 to 7.7 GPa and temperature range 1500 to 1800^{0}C for 30 to 180 s. During an experiment, load was applied corresponding to the desired pressure and the required power was fed

to the system. After the sintering time, the power was reduced to zero and then the pressure was released. The pressure-temperature-time conditions were varied to obtain the wBN - cBN composites with different volume fraction of cBN phase. The sintered compacts can be obtained in various sizes and shapes. The phase composition of the sintered compacts was determined by X-ray diffraction. The X-ray diffractogram of the starting wBN powder is shown in Fig. 5 and, the interplanar spacings of the different boron nitride modifications are given in Table 2. The extent of wBN→cBN transformation is estimated from the observed angular separation and relative intensities of the composite cBN (111)/ wBN (002) and wBN (100) peaks[15].

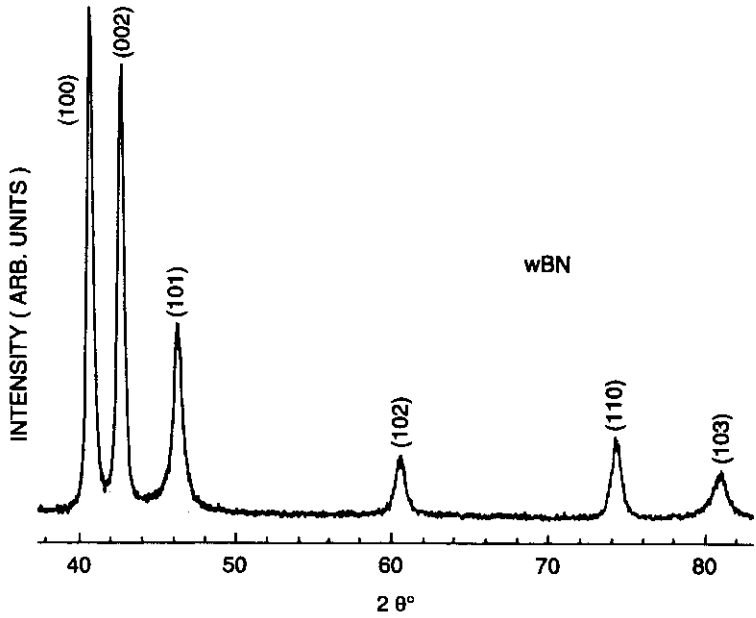

Figure 5: *X-ray diffractogram of wBN powder.*

During pressurization, the wBN particles undergo intense comminution due to the action of high static pressures[50–52]. The intensity of comminution increases with the increase in starting particle size. The isothermal holding at the sintering temperature at a particular pressure shows that comminution also takes place during sintering. Increase in the isothermal holding duration brings about recrystallization which leads

Table 2: Powder diffraction patterns of various modifications of boron nitride (Refs.15 and 49).

Phase	*hkl*	$d(A^0)$	*I*	$2\theta^0$ CuK_α
gBN	002	3.331	S	26.76
wBN	100	2.21	S	40.80
wBN	002	2.115	M	42.74
cBN	111	2.09	S	43.40
wBN	101	1.96	M	46.30
cBN	200	1.81	W	50.40
wBN	102	1.52	W	60.90
cBN	220	1.28	M	74.00
wBN	110	1.276	M	74.30
wBN	103	1.183	M	81.30
wBN	112	1.09	W	89.90
cBN	311	1.09	W	89.90

to the wBN→cBN transformation. The cBN formation in wBN is determined by the combined action of the hot plastic deformation and dynamic relaxation process via fragmentation, polygonization, primary and collective recrystallization[53–55]. During synthesis, after the release of pressure a certain fraction of wBN instantaneously transforms to gBN. Therefore, the final sintered compact is a dense body having a composite structure of wBN and cBN with finely dispersed gBN phase (2 - 7 vol. %). The microstructures of the sintered compacts are shown in Figs.6-8. The plastic deformation in the wBN phase during the early stage of sintering (7.7 GPa, 1800°C, 30 s), results in the formation of a microstructure shown in Fig. 6. In the wBN - cBN stability region, the increase in the sintering time leads to the increase in the cBN content in the compacts. The wBN→cBN transformation was almost complete when the sintering was carried out at 7.7 GPa and 1800°C for 180 s (Fig.7). The

Fig.6 (a)

Fig.6 (b)

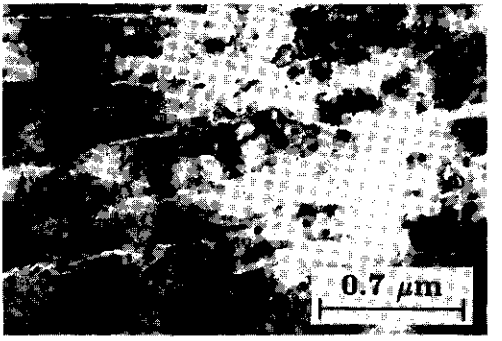

Fig.7

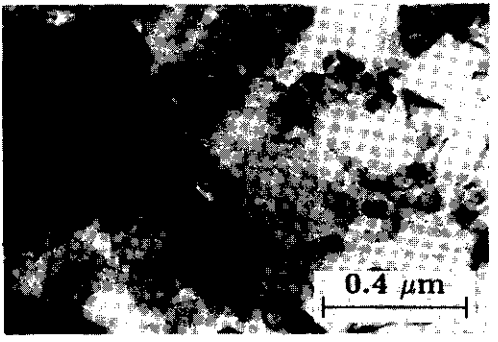

Fig.8

Figure 6: *Microstructure of P-T treated specimen. P - 7.7 GPa, T- 1800 ^{0}C, time - 30 s, (a) Fractograph and (b) Transmission micrograph showing hot plastic deformation of wBN grains.*

Figure 7: *Transmission electron micrograph of P-T treated specimen. P - 7.7 GPa, T- 1800 ^{0}C, time - 180 s, showing mostly cBN phase.*

Figure 8: *Transmission electron micrograph of composite (60 vol.% cBN) under intermediate sintering conditions.*

intermediate pressure and temperature conditions resulted in the formation of the two phase wBN-cBN composite structure (Fig.8). The wBN to cBN transformation being a diffusion controlled process, the grains of cBN coarsen with the increase in sintering time. The grains of the cubic phase (0.1 to 0.4μm) are at least one order of magnitude larger than the wBN grains($\ll 0.1\mu$m)[56] and can be easily identified in the microstructure.

A comparison of the various steps involved in the production of the composite and PCBN tools (Fig.3) shows that the cost of the PCBN tools will be higher than those of the composite. This is because, the production of PCBN tools requires cBN powder as the starting material, which itself has to be synthesized at high pressures and temperatures.

5 Properties of wBN - cBN composite

The mechanical properties of the wBN-cBN composite are dependent on the volume fraction of the cBN phase present in it. Various studies[57–63] on hardness, compressive stress, maximum internal stress, fracture energy and tool wear resistance have shown that the composite with 45 to 55 vol.% cBN has the optimum properties. The hardness of the composites varies from 30 to 70 GPa depending on the volume fraction of cBN present in them. The hot hardness of the optimum composite varies from 70 GPa at room temperature to 20 GPa at 1400 K. The indentation fracture toughness [64] values of the compacts are in the range 13-16.5 MPa$\sqrt{m}$.

The X-ray diffraction studies (line widths and macro-stresses) [60] on the sintered compacts have shown that the two phase polycrystals have residual stresses up to 2 GPa, whereas, the single phase compacts are almost free from these stresses. The Vickers hardness determined at a load of 50 N also showed a broad maximum (40 GPa) for the optimum composite. The effective energy of fracture of the composite (60 J m^{-2}) is an order of magnitude greater than the theoretical value of the surface energy (2 J m^{-2}).

The high toughness of the wBN - cBN composite can be explained in terms of (a) the fine grained structure of the composite, (b) the macro- and micro-stresses which are set up due to the differences in Young's moduli, volume compression moduli, coefficient of thermal expansion, the anisotropy in elastic properties of the wBN lattice and the difference in the specific volumes of cBN and wBN phases and (c) the transformation toughening due to the wBN $\rightarrow$ gBN transformation. Superhard

materials, in general, follow classic Griffith-type fracture with failure initiating from the preexisting flaws in the microstructure. In fine grained material, where critical flaw size (C_f) > grain size (d) , the fracture process is controlled by the additional energy being expended in the stage of formation and subcritical growth of the crack. In coarser grained material, where $C_f <$ d , there is no subcritical crack growth stage and therefore, the work done during crack formation and growth is negligible. Because of this, fine grained superhard materials exhibit higher fracture toughness than the coarse grained ones. On the application of external load, micro-cracks initiated by the residual stresses promote stress relaxation at the tip of the crack thereby imparting high fracture toughness in this material. The additional toughening mechanism in the wBN-cBN composite is similar to the transformation toughening mechanism operating in metastable zirconia ceramics[65,66]. The graphitization that occurs during the release of pressure after sintering results in an increase of specific volume which sets up compressive stresses around the transformed gBN particles. This leads to rounding of the propagating crack tips and micro-crack formation which impede crack propagation[57]. The formation of micro-cracks is also assisted by the highly anisotropic fracture behaviour of the gBN due to easy cleavage perpendicular to c-axis.

A comparison of the various properties of wBN-cBN composite with tungsten carbide (K_{20}), PCD, amborite (amber boron nitride particles with metallic binder), DBC50 (finer cBN particles dispersed in TiC with aluminium diboride and nitride) are given in the Table 3. It can be seen that the fracture toughness of composite is very high, as compared to those of diamond and cBN based materials and similar to that of WC-10 Co cemented carbide.

6 Applications

The main application of the composite tool is in the machining of hardened steels, cast irons, hard alloys and other difficult-to-cut materials. The distinguishing feature of the composite tool is its capacity to operate under impact loads during machining operation. The economic use of polycrystalline boron nitride tool in machining hard ferrous alloys (over HRC 45) is based on the principle of self induced hot machining. In conventional tool materials, it is a standard practice to employ positive rake angle and low cutting speeds to reduce the cutting temperatures and forces. In contrast, superhard material tools require negative rake angle and relatively higher cutting

speeds. The negative rake angle, together with the high cutting speed, generates heat which continuously softens the work piece in the small volume of the cutting zone. The temperatures generated at the shear zone are high enough for the cutting edge and the chips to become red hot. The softening of the work-material, due to heat

Table 3: Physical and mechanical properties of hard materials (* Ref: 49,67,68; † Ref :69; ‡ Ref :70)

Property	K_{20}†	PCD-10†	Amborite†	DBC-50‡	Composite*
Density (gcm^{-3})	14.70	4.12	3.42	-	3.39-3.44
Compressive Strength (GPa)	4.50	7.60	2.73	-	3-4
Bending Strength (GPa)	2.07	1.26	0.57	-	1.20
Fracture Toughness ($MPa\sqrt{m}$)	10.80	7.30	6.30	3.70	13-16
Knoop Hardness (GPa)	13	50	32	28	30-70
Young's Modulus (GPa)	620	776	680	587	760
Coefficient of Thermal Expansion ($10^{-6}K^{-1}$)	5.4	4.2	4.9	4.7	2.7 3.7
Thermal Conductivity ($Wm^{-1}K^{-1}$)	100	560	100	44	40-50

generated by the friction and intense shear strain, makes it possible to machine high speed steel harder than HRC 60 continuously for long periods. The heat generated is taken away by the chip or the tool which has a high thermal conductivity (40-50 $Wm^{-1}K^{-1}$). The work piece, therefore, remains cool and its hardness is not affected.

7 Performance of composite tools

The performance of the composite tools in the machining of hardened steel components have been conducted as a function of cBN content in them[61,67]. It has been reported , that the tools with large amount of cBN perform very well in continuous machining, whereas, the composite with 45-55% cBN performs best in interrupted

machining conditions. A comparative study[71] on the composite and a variety of PCBN tools (Amborite, Niborite, Sumiboron etc.) has indicated that the tool life is longer in case of the composite tool as compared to those of PCBN tools while machining hardened steels.

Machining tests have been conducted in the present study with composite tools on various work materials. The experimental methods adopted and the results obtained are summerized below.

7.1 Machining tests and results

The wBN - cBN compacts obtained by high pressure - high temperature sintering were metallized and brazed onto steel holders. The tool tips were ground to the required geometry using diamond wheels. The tool geometry used in the present investigation is as follows: clearance angle = 12^0, rake angle = - 11^0, end relief angle = 15^0, plan approach angle = 45^0 and nose radius = 0.3 - 0.4 mm.

The work materials used for the machining tests were hardened tool steel (HRC 60-63), hardened alloy steel (HRC 40-43), high nickel cast iron (BHN 120-160) and Ti-6Al-4V alloy (HV 310).

The turning tests were conducted to evaluate the tool life and the surface finish on the job. The work piece was centered at one end and mounted between a three jaw chuck and tail-stock rotating center. The surface layer of the heat treated test pieces was removed before the commencement of tests. The tools were mounted in a quick-change tool post, care being taken to ensure that the unsupported length was identical for all tools under test. The machining conditions employed are given in Table 4. The tool life was determined by measuring the flank wear width (V_B) of the tool. The tool life criterion was set to V_B = 0.40 mm . The flank wear width was obtained by determining the mean distance between the initial cutting edge and the front of the worn portion of the tool. The tool post was removed from the machine after predetermined time intervals and the wear on the tool was measured with the help of a microscope equipped with graticule (least count of 0.047 mm). Tests were also carried out under interrupted cutting conditions by providing a 5 mm wide axial slot in the work piece.

Machining tests were carried out with the commercially available cemented carbide tools for a comparative study. WIDIA P_{30} grade cemented carbide tools were

Table 4: Performance of composite tools

Machining conditions, Tool life and Surface finish	Work material/tool			
	Tool steel Composite	EN24 Composite/P_{30}	Cast iron Composite/K_{20}	Ti alloy Composite/K_{20}
Speed (m/min.)	80	80/60	340/80	75
Feed (mm/rev.)	0.075	0.075	0.1	0.1
Depth of cut (mm)	0.2	0.2	0.5	0.5
Fluid*	not used	not used/used	not used	used
Life(min)				
Continuous	138	108		80/12
Interrupted	135			
Surface finish				
R_a (μm)	1.25	0.85	0.45/2.65	1.08/1.52
R_t (μm)	2.43	7.39	4.82/15.74	7.83/10.6

* Water based coolant

used for machining hardened EN 24. A synthetic cutting fluid was used during the test. Dry machining of cast iron was conducted using WIDIA K_{20} grade cemented carbide tools. Wet machining of the titanium alloy was conducted using WIDIA K_{20} grade carbide tools. The cutting conditions employed are given in the Table 4.

The variation of flank wear with time while machining tool steel in interrupted cutting is shown in Fig 9. It shows three distinct regions in the flank wear, V_B , versus time plot: (i) initial rapid wear followed by (ii) a steady and slow wear, and finally (iii) a steep increase in wear rate. The quality of the machined surface (R_a and R_t values) obtained while machining with the composite and carbide tools are presented in Table 4. It can be seen that the surface finish obtained with composite tools is always better than that with cemented carbide tools. The SEM pictures of the worn tool while machining titanium alloy are shown in Fig 11.

7.2 Wear characteristics

The various types of wear that can take place in a turning tool are shown schematically in Fig 10. At the cutting edge, wear is normally observed on the rake face and flank surface. Wear on the rake is characterized by the formation of crater which results due to the flow of the chip along the face. Wear on the flank is caused by the abrasion of the freshly cut surface. At low cutting speeds, the flank wear rate is faster than the crater wear. The abrasion resistance of a tool is often related to its hardness. The abrasive wear is minimized if the hot hardness of the tool in the cutting temperature range is greater than the hardness of the hard particles present in the work piece. At higher cuttung speeds, the crater wear takes place mainly due to the chemical instability of the tool material - work piece combination at elevated temperatures.

Fig.9

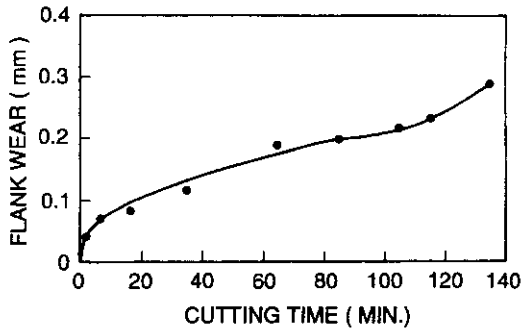

Fig.10

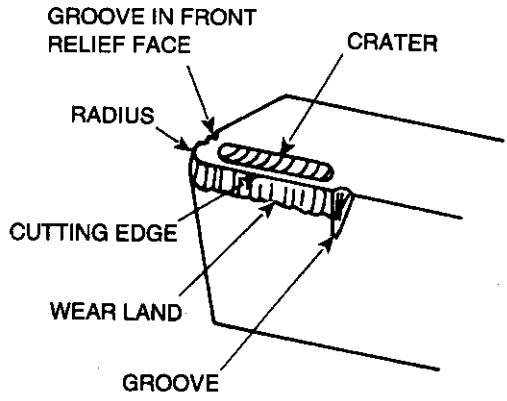

Figure 9: *The variation of flank wear with time while interrupted machining of hardened tool steel (HRC 60-63) with composite tools. Machining conditions: speed- 70 to 80 m/min, feed- 0.075 mm/rev, depth of cut -0.2mm (Ref.11).*

Figure 10: *Schematic diagram of different wear zones on a turning tool.*

Hardened steel and cast iron

Our earlier studies[11] on the wear characteristics of the composite tools while machining ferrous alloys have shown that the wear on the tool occurs in various

stages. In the initial few seconds of machining, microspalling occurs resulting in the rounding of the cutting edge. Once proper contact between the tool and the work piece is established, a wear band is formed on the flank. On continued cutting, the crater which develops on the rake deepens and increases the rake angle in the positive direction. This weakens the tool and leads to further microspalling. Under favourable conditions, the wear bands disappear during the microspalling and the wear cycle is repeated.

In interrupted cutting, the wear on the tool takes place by the formation of cracks, which are generated due to thermal and mechanical fatigue . Thermal cracks are formed due to large temperature gradient and temperature fluctuation during cutting and non-cutting periods. They form either on the rake or on the flank or on both in the direction perpendicular to the cutting edge. Such cracks are not observed in composite tools. The high thermal shock resistance of the composite tools can be attributed to their high thermal conductivity and fracture toughness. However, cracks on the flank parallel to cutting edge were observed which are normally associated with the mechanical fatigue.

In cast iron machining, the wear on the tool is due to the formation of grooves close to the major cutting edge. In steel machining, there is a continuous chip formation and the maximum temperature is generated on the rake face away from the cutting edge. Whereas, in cast iron machining, the chip is segmented and the highest temperature is generated closer to the cutting edge. In addition, the temperature on the flank face may be equal to or even more than the temperature on the rake face. This unfavourable temperature distribution and the high abrasiveness of cast iron leads to groove formation on both rake and flank face.

Titanium alloy

The machining of titanium alloys is difficult basically due to its high chemical affinity and the high local temperature generated because of its poor thermal conductivity (8 W $m^{-1}K^{-1}$). The progress of flank wear on the composite tool is as follows : After following a rapid initial wear, the wear rate reaches a steady state after about 5 min.. The wear rate shows a tendency to increase after 50 min. The typical SEM pictures of the worn rake face of the composite tool after 10, 50 and 80 min. of machining are shown in Fig.11. The tool shows the formation of an adherent layer along the cutting edge (Figs.11 a and b). This layer is due to the

chemical reaction between titanium and, the boron and nitrogen present in the tool material. On further cutting, the layer becomes thick and grows perpendicular to the cutting edge. The tool after 50 minutes of machining shows the fracturing of the layer formed earlier (Fig.11 c). The tool after 80 minutes of machining shows the formation of groove on the rake face (Fig. 11 d). The crater wear on the tool is large compared to the flank wear and causes failure of the tool, before a critical value of V_B is reached.

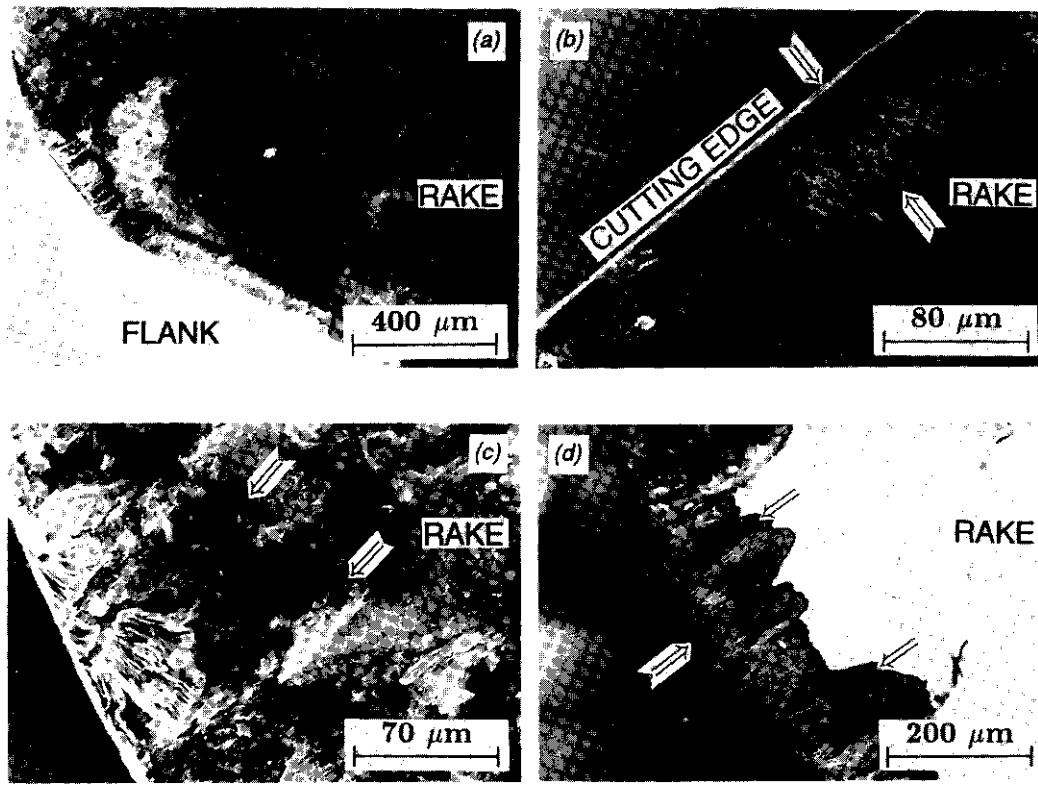

Figure 11: *SEM micrographs of the worn tools while machining titanium alloy. (a) Formation of the reaction layer, (b) Magnified view of the layer, (c) Plucking of hard particles (marked with arrows) and (d) Formation of grooves.*

When the reaction layer is detached with the chip, hard particles from the tool may be plucked causing the groove and deepening the crater. During this process,

the resistance to plastic deformation of the tool material at elevated temperatures comes into picture. A similar attrition wear on the flank leads to the weakening of the cutting edge and failure of the tool occurs. The fracture toughness of the tool material plays an important role during this period in delaying the fracture of the tool. Thus the high hot hardness and the fracture toughness of the composite contribute to the success of this tool.

7.3 Comparative performance of composite and cemented carbide tools

The results of the machining tests conducted on heat treated alloy steel (HRC 40-43) and high nickel cast iron (BHN 120-160) and the titanium alloy with composite and cemented carbide tools are summarized in Table 4. In machining hardened EN 24, the tool life with composite was more than cemented carbide by at least a factor of 2 even with a higher cutting speed. Furthermore, the surface finish of the workpiece achieved with the composite was always better than that with cemented carbide. In case of composite, the R_a values remained in the range 0.85-1.00μm even at a V_B of 0.38 mm, whereas, the best surface finish obtained with cemented carbide was about 2.30μm (R_a). It is evident from Table 4 that composite tool can machine cast iron at a much higher speed than cemented carbide (a factor of 4-5). Even at this high cutting speed, the surface finish obtained was 0.45μm (R_a) as compared to 2.65μm (R_a) with cemented carbide after about 15 minutes of machining. Secondly, the depth of surface roughness (R_t) obtained in case of cemented carbide was very large (15-20μm) as against 4.82μm with composite tools. In machining titanium alloys also the superiority of the composite tool is clear. The composite tools continued to work for 80 minutes whereas the carbide tools failed after 12 minutes. The surface finish obtained was significantly better with the composite (R_a-1.08μm after 80 min.) than with the carbide tools (R_a-1.52μm after 12 min.).

8 Conclusions

The wBN-cBN composite has an excellent combination of hardness, toughness and relative chemical stability. The composite tools can be used economically in the machining of hardened steels, cast irons and titanium alloys. The wear of the tools in machining titanium alloy can be associated with the chemical interactions between the tool and the work piece. The high fracture toughness of these tools allows them to be used on non rigid machines.

Acknowledgements

This work was done under ILTP, and the authors thank Dr. P.Rama Rao, Prof. R.Narasimha and Dr K.N.Raju for their constant help and encouragement. The authors are grateful to Academician V.I.Trefilov and Prof. A.V.Bochko of IMSP, Kiev for providing facilities for sintering studies and the cutting tools for the performance studies. The help received from Mr. T.Irudaya Raj, Mr. P.M.Jaman and Mr. C Swamy in conducting the machining trials is gratefully acknowledged.

References

1. Materials Sci. and Engg. for the 1990's, *National Research Council*, **25**, (1990).
2. R.H.Wentorf, *J.Chem.Phys.*, **26**, 956 (1957).
3. H.P.Bovenkerk, F.P.Bundy, H.T.Hall, H.M.Strong and R.H.Wentorf, *Nature*, **184**, 1094 (1959).
4. R.H.Wentorf, *J.Chem.Phys.*, **34**, 809 (1961).
5. L.Vel, G.Damazeau and J.Etourneau, *Mat.Sci.and Engg.*, **B10**, 149 (1991).
6. P.N.Tomlinson and R.J.Wedlake, *Speciality steels and hard materials*, Eds. N.R.Comins and J.B.Clark, Pergamon press, New York, (1983) p-173.
7. H.J.Modi, *Workshop on high pressure techniques in metal forming and materials synthesis*, (1985).
8. S.K.Bhaumik, C.Divakar, A.K.Singh and A.V.Bochko *Metals, Materials and Processes.* **5**, 199 (1993).
9. V.I.Trefilov, I.N.Frantsevich et al, *Sint.Almazy*, **4**, 24 (1974).
10. C.Divakar, S.K.Bhaumik and A.K.Singh *Metals, Materials and Processes*, (in press)
11. S.K.Bhaumik, C.Divakar and A.K.Singh, *Metals, Materials and Processes*, (in press).
12. A.V.Kurdyumov, A.N.Pilyankevich and I.N.Frantsevich, *Poroshkovaya Metallurgiya*, **10**, 57 (1973).
13. A.Verma and P.Krishna, *Polymorphism and Polytypism in Crystals*, Wiley (1966).
14. F.P.Bundy and R.H.Wentorf, *J.Chem.Phys.*, **38**, 1144 (1963).
15. F.R.Corrigan and F.P.Bundy, *J.Chem.Phys.*, **63**, 3812 (1975).
16. M.Wakatsuki, K.Ichinose and T.Aoki, *Mat.Res.Bull*, **7**, 999 (1972).
17. K.Ichinose, M.Wakatsuki, T.Aoki and Y.Maeda, *Proc. 4 AIRAPT Conf.*, Ed. J. Osugi, Kawakita Printing Co. Ltd., Kyoto, (1975) p-441.
18. M.Wakatsuki, K.Ichinose, *Prof. 4 AIRAPT Conf.*, Ed. J. Osugi, Kawakita Printing Co. Ltd., Kyoto, (1975) p-436.
19. M.Wakatsuki, K.J.Takano and G.Fujita, *Physica*, **139 and 140 B**, 256 (1986).
20. L.F.Vereschagin, E.V.Zubova, L.N.Burenkova and N.I.Revin, *Dokl.Akad. Nauk SSSR*, **178**, 72 (1968).

21. L.V.Al'tshuler, M.N.Pavlovskii and V.P.Drakin, *Zh.Eksperim.i.Teor.Fiz*, **52**, 400 (1967).
22. G.A.Adadurov, Z.G.Aliev, L.O.Atovmyan, T.V.Bavina, Yu G. Borod'ko, O.N. Breusov, A.N. Dremin, A.Kh. Muranevich and S.V. Pershin, *Dokl.Akad.Nauk. SSSR*, **172**, 1066 (1967).
23. P.S.DeCarli, *Bull.Am.Phys.Soc.*, **12**, 1127 (1967).
24. N.L.Coleburn and J.W.Forbes, *J.Chem.Phys.*, **48**, 555 (1968).
25. Q.Johnson and A.C.Mitchell, *Phys.Rev.Lett.*, **29**, 1369 (1972).
26. T.Soma, A.Sawaoka and S.Saito, *Mat.Res.Bull*, **9**, 755 (1974).
27. T.Soma, A.Sawaoka and S.Saito, *Proc. 4 AIRAPT Conf.*, Ed. J. Osugi, Kawakita Printing Co. Ltd., Kyoto, (1975) p-446.
28. M.Wakatsuki and K.Ichinose, *Proc. 4 AIRAPT Conf.*, Ed. J. Osugi, Kawakita Printing Co. Ltd., Kyoto, (1975) p-441.
29. S.Saito and A.Sawaoka, *High Pressure Sci. and Tech.*, **1**, 986 (1979).
30. S.Saito and A.Sawaoka, *High Pressure Sci and Tech.*, **1**, 541 (1980).
31. T.Sekine, *J.Mat.Sci.Lett.*, **8**, 872 (1989).
32. R.S.Devries and J.F.Fleischer, *Mat.Res.Bull.*, **4**, 433 (1969).
33. K.Susa, T.Kobayashi and S.Taniguchi, *Mat.Res.Bull.*, **9**, 1443 (1974).
34. T.Endo, O.Fukunaga and M.Iwata, *J.Mat.Sci.*, **14**, 1375 (1979).
35. T.Kobayashi, *J.Chem.Phys.*, **70**, 5898 (1979).
36. T.Kobayashi, *Mat.Res.Bull.*, **14**, 1541 (1979).
37. T.Endo, O.Fukunaga and M.Iwata, *J.Mat.Sci.*, **14**, 1676 (1979).
38. T.R.Balan, A.V. Kurdyumov, N.F. Ostrovskaya and A. N. Pilyankevich, *Dokl. Acad. UkrSSR.*, **12**, 1109 (1976).
39. A.V.Kurdyumov, *Poroshkovaya Metallurgiya*, **12**, 69 (1975).
40. A.V.Kurdyumov, N.F.Ostrovskaya, V. A. Pilipenko and A. N. Pilyankevich, *Poroshkovaya Metallurgiya*, **9**, 76 (1978).
41. A.V.Kurdyumov, N.F.Ostrovskaya, A. N. Pilyankevich, T. R. Balan and A. V. Bochko *Poroshkovaya Metallurgiya*, **1**, 64 (1976).
42. L.F.Vereschagin, V.A.Galaktionov, A. A. Semerchan and V. N. Slesarev, *Dokl. Akad. Nauk SSSR*, **132**, 1059 (1960).
43. H.T.Hall, *Rev.Sci.Instrum.*, **31**, 125 (1960).
44. H.T.Hall, *Rev.Sci.Instrum.*, **29**, 267 (1958).
45. A.Zeitlin, *Mech.Engg.*, **83**, 37 (1961).
46. A. Zeitlin and J. Brayman, *High pressure measurements*, Ed. A. A. Giardini and E. C. Lloyd, Butterworths, 301 (1963).
47. H.T.Hall, *Rev.Sci.Instrum.*, **33**, 1278 (1962).
48. L.F.Vereschagin, L.G.Khvostantev and A.P.Novikov, *High Temp-High Press.*, **9**, 637 (1977).
49. A.V.Kurdyumov and A.N.Pilyankevich in *Phase transformations in carbon and boron nitride (Russian)*, (1979).

50. S.S.Dzhamarov, *Poroshkovaya Metallurgiya*, **6**, 238 (1982).
51. S.S.Dzhamarov and N.I.Schcherban, *Poroshkovaya Metallurgiya*, **2**, 32 (1983).
52. M.S.Kovalchenko and S.S.Dzhamarov, *Poroshkovaya Metallurgiya*, **2**, 31 (1984).
53. I.N.Frantsevich and T.R.Balan, *Dokl.Acad.Nauk SSSR*, **218**, 591 (1984).
54. A.V.Kurdyumov, *Poroshkovaya Metallurgiya*, **1**, 64 (1976).
55. A.V.Kurdyumov, *Poroshkovaya Metallurgiya*, **4**, 96 (1986).
56. A. V. Kurdyumov, G. S. Oleinik, A. N. Pilyankevich, T. R. Balan, A. V. Bochko and S. S. Dzhamarov, *Poroshkovaya Metallurgiya*, **10**, 47 (1976).
57. A. V. Bochko, O. N. Grigoriev, S. S. Dzhamarov, G. G. Karyuk, Yu. V. Milman and V. I. Trefilov, *Poroshkovaya Metallurgiya*, **6**, 4 (1977).
58. A. V. Bochko, O. N. Grigoriev, S. S. Dzhamarov, G. G. Karyuk, A. V. Kurdyumov, G. S. Oleinik, A. N. Pilyankevich, V. I. Trefilov, I. N. Frantsevich and A. N. Shatokhin, *Poroshkovaya Metallurgiya*, **10**, 61 (1979).
59. A. V. Bochko, O. N. Grigoriev, S. S. Dzhamarov, A. N. Pilyankevich, V. I. Trefilov, G. G. Karyuk, I. N. Frantsevich and A. N. Shatokhin, *Poroshkovaya Metallurgiya*, **5**, 96 (1980).
60. O. N. Grigoriev, S. S. Dzhamarov, V. I. Trefilov, and A. N. Shatokhin, *Poroshkovaya Metallurgiya*, **1**, 53 (1981).
61. O.N.Grigoriev, S.S.Dzhamarov, V.I.Trefilov, and A.N.Shatokhin, *Diamond Superhard Material*, **7**, 4 (1981).
62. A.V.Bochko, O.N.Grigoriev, T. M. Svyazkina and A. M. Shatokhin, *Poroshkovaya Metallurgiya*, **4**, 87 (1986).
63. V.I.Trefilov, Yu.V.MilMan and O.N.Grigoriev, *Prog.Crystal Growth and Charact.*, **16**, 225 (1988).
64. A.G.Evans and E.A.Charles, *J.Am.Ceram.Soc.*, **59**, 371 (1977).
65. A.N.Pilyankevich and N.Claussen, *Mat.Res.Bull.*, **13**, 413 (1978).
66. N.Claussen, *J.Am.Ceram.Soc.*, **61**, 85 (1978).
67. G.G.Karyuk, A.V.Bochko, V.V.Yarosh, S. S. Dzhamarov, V. M. Volkogon and A. O. Aronovich, *Proc.XI AIRAPT Conf.*, Vol.2, 128 (1989).
68. V.L.Primachuk, A.V.Bochko and A.O.Avetisyan, *Poroshkovaya Metallurgiya*, **8**, 80 (1983).
69. P.K.Bossom, *Ind.Dia.Rev.*, **50**, 228 (1990).
70. R.M.Hooper, J.I.Shakib, A.Parry and C.A.Brookes, *Ind.Dia.Rev.*, **49**, 170, (1989)
71. G. G. Karyuk, A. V. Bochko, V. M. Volkogon, S. S. Dzhamarov, P. V. Zhakarenko and V. S. Sil'vestrov, *Poroshkovaya Metallurgiya*, **8**, 92 (1987).